Structure of the dimeric RC-LH1-PufX complex from Rhodobaca bogoriensis investigated by electron microscopy

Semchonok, Dmitry A.; Chauvin, Jean-Paul; Frese, Raoul N.; Jungas, Colette; Boekema, Egbert J.

Published in:
Philosophical Transactions of the Royal Society of London. Series B: Biological Sciences

DOI:
10.1098/rstb.2012.0063

Publication date:
2012

PHILOSOPHICAL TRANSACTIONS OF THE ROYAL SOCIETY B

CrossMark click for updates

Phil. Trans. R. Soc. B (2012) **367**, 3412–3419
doi:10.1098/rstb.2012.0063

Research

Structure of the dimeric RC–LH1–PufX complex from *Rhodobaca bogoriensis* investigated by electron microscopy

Dmitry A. Semchonok[1], Jean-Paul Chauvin[2], Raoul N. Frese[3], Colette Jungas[4,5,6,*] and Egbert J. Boekema[1,*]

[1]*Electron Microscopy Group, Groningen Biomolecular Sciences and Biotechnology Institute, University of Groningen, Nijenborgh 7, 9747 AG, Groningen, The Netherlands*
[2]*IBDML – Developmental Biology Institute of Marseille Luminy, Aix-Marseille Université, UMR 7288, Case 907 – Parc Scientifique de Luminy, 13288 Marseille Cedex 9, France*
[3]*Biophysics, VU University, De Boelelaan 1084, Amsterdam, The Netherlands*
[4]*Lab Bioenerget Cellulaire, CEA, IBEB, 13108 Saint-Paul-lez-Durance, France*
[5]*UMR 7265 Biologie Végétale et Microbiologie Environnementales, CNRS, 13108 Saint-Paul-lez-Durance, France*
[6]*Aix-Marseille Université, 13108 Saint-Paul-lez-Durance, France*

Electron microscopy and single-particle averaging were performed on isolated reaction centre (RC)—antenna complexes (RC–LH1–PufX complexes) of *Rhodobaca bogoriensis* strain LBB1, with the aim of establishing the LH1 antenna conformation, and, in particular, the structural role of the PufX protein. Projection maps of dimeric complexes were obtained at 13 Å resolution and show the positions of the 2 × 14 LH1 α- and β-subunits. This new dimeric complex displays two open, C-shaped LH1 aggregates of 13 αβ polypeptides partially surrounding the RCs plus two LH1 units forming the dimer interface in the centre. Between the interface and the two half rings are two openings on each side. Next to the openings, there are four additional densities present per dimer, considered to be occupied by four copies of PufX. The position of the RC in our model was verified by comparison with RC–LH1–PufX complexes in membranes. Our model differs from previously proposed configurations for *Rhodobacter* species in which the LH1 ribbon is continuous in the shape of an S, and the stoichiometry is of one PufX per RC.

Keywords: light-harvesting complex; *Rhodobaca bogoriensis*; purple bacteria; LH1; PufX; electron microscopy

1. INTRODUCTION

In purple non-sulphur photosynthetic bacteria, the primary reactions of photosynthesis are carried out by an RC–LH1 complex formed by the photochemical reaction centre (RC) and the LH1 light-harvesting pigment-protein. Many species have additional peripheral antenna complexes, such as LH2, to increase the light-harvesting capacity and to transfer that energy rapidly and efficiently to the RCs initiating charge separation. Both LH1 and LH2 are constructed on a modular principle. The functional module or unit appears to be a heterodimer of two low-molecular-weight subunits with a single α helix, called α and β. One α–β dimer binds 2–3 bacteriochlorophyll *a* (Bchl *a*) molecules and 1–2 carotenoids. Multiple copies of such units form ring-like LH1 and LH2 complexes (see [1] for a review).

* Authors for correspondence (colette.jungas@cea.fr; e.j.boekema@rug.nl).

One contribution of 16 to a Theo Murphy Meeting Issue 'The plant thylakoid membrane: structure, organization, assembly and dynamic response to the environment'.

LH2 rings are single entities without a fixed structural interaction with the other photosynthetic proteins, whereas LH1 rings encircle the RC. Biochemical experiments, electron microscopy (EM) and atomic force microscopy (AFM) investigations have shown that the supercomplex of RC–LH1 can exist as a monomer or a dimer in the native membrane. Monomeric RC–LH1 complexes are assembled in most of the species, such as *Blastochloris* (*Blc.*) *viridis* [2], *Rhodopseudomonas* (*Rps.*) *palustris* [3], *Phaeospirillum molischianum* [4], *Rhodobacter* (*Rba.*) *veldkampii* [5,6], *Rps. rubrum* [7], *Rba. capsulatus* and *Rba. vinaykumarii* [8], whereas a dimeric form is assembled in *Rba. sphaeroides* [9–11], *Rba. blasticus* [12], *Rba. changlensis* and *Rba. azotoformans* [8], in which two RCs are surrounded by an S-shaped ribbon of LH1 antenna units. In species where both monomers and dimers exist, the ratio between them depends on light intensity [8].

The RC of *Blastochloris viridis* was the first membrane protein solved at a high resolution [13]. The RC of purple bacteria consists of three major subunits, H, M and L, with a total of 11 transmembrane helical

segments. In some purple bacteria, a fourth subunit, cytochrome *c*, is associated with the complex at the membrane surface. The L and the M subunits are paired transmembrane proteins with 2×5 transmembrane α helices that together form a cylindrical structure with roughly bilateral symmetry about its long axis. The H subunit is anchored to the membrane by a single transmembrane α helix. There are no high-resolution data of a dimeric RC–LH1 complex, but a 4.8 Å-resolution structure is available for the monomeric RC–LH1 from *Rps. palustris* [3]. The RC–LH1 structure shows the RC surrounded by an oval LH1 complex, which consists of 15 pairs of transmembrane helical α and β-apoproteins and their coordinated bacteriochlorophylls. Complete closure of the RC by the LH1 is prevented by the association of a small protein, consisting of a single transmembrane helix, out of register with the array of inner LH1 α-apoproteins [3]. This protein was called protein W in this specific case, and turned later on to be PufX in the *Rhodobacter* genus (reviewed in Holden-Dye *et al.* [14], see also below). It induces an opening in the LH1 ring, located next to the binding site in the RC for the secondary electron acceptor ubiquinone [3]. The opening allows passage of quinones, involved in electron transfer, to come in contact with the RC where they are photoreduced and protonated [9].

The structure of RC–LH1 dimers has been investigated by EM and AFM. The highest resolution data concern a 8.5 Å projection structure derived from two-dimensional crystals [11]. The two-dimensional map reveals the α-helical structure of two reaction centres and 28 LH1 units. This work was extended with a low-resolution three-dimensional structure [15]. A special feature of the dimer, found in this study, is its kinked conformation. The intrinsic curvature of the dimer at least partially accounts for the shape and 70-nm diameter of spherical membrane invaginations, known as intracytoplasmic membrane vesicles or chromatophores in wild-type *Rba. sphaeroides* [16].

The PufX protein interacts with the LH1 α-subunits of the RC–LH1 complex [17]. Because PufX is strictly required for the isolation of dimeric RC–LH1 complexes, it was suggested that it has a central structural role in dimer formation [18]. Because high-resolution data are lacking, the precise location of PufX within the dimers is not yet firmly established. On the basis of an 8.5 Å projection structure, PufX was proposed to be localized near the centre of the RC–LH1 dimer, within the ring of the LH1 units [11]. This model was refined after establishing the PufX solution structure by NMR [19]. The NMR study suggests that the membrane-spanning helix of PufX adopts a bent conformation. The N-terminal part of PufX was found to be critical for the formation of dimers of the RC–LH1 and, in the refined dimer model, the N-termini of the two PufX proteins point to the interface between the monomers. In a second type of model, PufX is placed at the dimerization interface in the centre of the dimer complex and is itself also thought to be dimerized [5,10,12]. In another model, the two PufX molecules are also placed in the centre of the dimer, but not in close contact [8]. A combination of computational and experimental techniques was used to test the hypothesized homodimerization of PufX. Results suggest that the different oligomerization states of monomeric complexes in various species can be attributed to, among other factors, the different propensity of its PufX helix to homodimerize [20]. Species with dimeric core complexes have a PufX that can potentially form a homodimer, whereas the one species with monomeric core complexes has a PufX with little to no dimerization propensity. This study, however, could not establish the PufX position.

In the present work, we investigated the structure of the dimeric RC–LH1 complex from *Rhodobaca* (*Rca.*) *bogoriensis* strain LBB1, an alkaliphilic non-sulphur purple bacterium found in African Rift valley soda lakes [21]. A full description of the biochemical characterization of these complexes will be published elsewhere. In this contribution, we focus on establishing the configuration of the peripheral LH1 antenna ring and PufX localization by single-particle averaging of EM projection of dimeric RC–LH1 complexes. Positions of α helices could be visualized in two-dimensional projection maps and show how LH1 units surround the RCs and form the dimer interface.

2. MATERIAL AND METHODS

(a) *Isolation of RC–LH1–PufX complexes*

Photosynthetic membranes were solubilized and purified using the method as described by Comayras *et al.* [22] with modifications (C. Jungas 2011, unpublished data). Freshly harvested cells were collected by low-speed centrifugation at 8000*g*, washed with 20 mM Tris–HCl (pH 8) and 1 mM 4-(2-aminoethyl) benzenesulfonyl fluoride (Interchim), and subjected to three cycles with French press at 16 000 p.s.i. The resulting unbroken cells and debris were removed by centrifugation at 20 000*g* for 30 min at 4°C. The photosynthetic membranes were then pelleted at 200 000*g* for 90 min and resuspended in 20 mM Tris–HCl (pH 8) and 1 mM 4-(2-aminoethyl) benzenesulfonyl fluoride. For the preparation of RC–LH1 complexes (see below), the membranes were treated with 3 M NaBr, followed by two washes with 50 mM Tris–HCl (pH 8) to remove membrane-attached proteins. In all experiments, the membranes were suspended in 20 mM Tris–HCl (pH 8.0).

Photosynthetic membranes were solubilized with 1 per cent *n*-β-dodecyl maltoside (Biomol) for 10 min at 4°C and then ultracentrifuged at 200 000*g* for 30 min to remove the insoluble material. The solubilized complexes were laid on a continuous density sucrose gradient, containing 20 mM Tris–HCl (pH 8), 0.5 M sucrose and 0.01 per cent *n*-β-dodecyl maltoside and ultracentrifuged at 200 000*g* for 15 h at 4°C. Three pigment-containing bands were thus separated and ascribed (from top to bottom) to bc_1 cytochrome, monomeric and dimeric RC–LH1 complexes. The latter fraction was carefully collected using a syringe and applied to a Mono Q anion exchange fast protein liquid chromatography column (GE Healthcare) pre-equilibrated with 50 mm Tris–HCl (pH 8) and 0.015 per cent *n*-β-dodecyl maltoside. After washing with 5 ml of buffer, the complexes were eluted with a 30 ml

linear gradient of 0–500 mM NaCl at a rate of 0.5 ml min^{-1}. The dimer fraction was collected and concentrated by gel filtration (Superose-6 column, GE Healthcare). The peak fraction was stored frozen in small aliquots for structural research.

(b) *Detection of PufX in* Rca. bogoriensis

The DNA fragment between the *pufM* (coding for the M subunit reaction centre) and *ORF641* genes was amplified by polymerase chain reaction (PCR) from *Rca. bogoriensis* according to the procedure in Tsukatani *et al*. [23]. The sequence analysis deduced from the translated PCR product confirms the presence of PufX. PufX was also identified by mass spectrometry (MS) analyses both by peptide mass fingerprint on a MALDI-ToF (33% sequence coverage) and by MS/MS on a nanoLC-Q-ToF mass spectrometer (17% coverage; data not shown).

(c) *Electron microscopy and image processing*

Samples of purified RC–LH1–PufX complexes were prepared for EM by negative staining with 2 per cent uranyl acetate on glow-discharged carbon-coated copper grids. EM was carried out on a Philips CM120 electron microscope equipped with a LaB_6 tip, operated at 120 kV. Images were recorded with a Gatan 4000 SP 4K slow-scan CCD camera at 133 000× magnification, compatible to a pixel size of 2.25 Å at the specimen level after binning the images to 2048 × 2048 pixels. GRACE software was used for semi-automated data acquisition [24]. In total, over 15 000 images were used for extracting 85 000 single-particle projections. Single-particle averaging was performed with Groningen image processing software, including reference alignments, classification and averaging of aligned projections. Resolution in projection maps was determined with the Fourier ring correlation method [25].

For fitting purposes, the high-resolution structure of the photosynthetic reaction centre from *Rba. sphaeroides* (Protein Data Bank entry: 1Z9k) was used. All distances, angles and areas were measured using the ImageJ program [26].

Freeze-fractured studies were conducted on whole cells grown photosynthetically. After overnight fixation with 2.5 per cent glutaraldehyde in 0.1 M cacodylate buffer pH 7.2, cells were exposed to increasing concentrations of glycerol in cacodylate buffer until a final concentration of 30 per cent glycerol was attained. The specimens were freeze-fractured at −110°C in a Balzers BAF 300 freeze etch unit and immediately shadowed with platinum/carbon at 3×10^{-6} Torr (1.3×10^{-4} Pa).

AFM on membranes of *Rba. sphaeroides* was performed in tapping mode on a home-built AFM [27]. For AFM, membranes were adsorbed for 30 min onto the surface of freshly cleaved mica within adsorption buffer: 10 mM Tris–HCl pH 7.5, 150 mM KCl, 25 mM $MgCl_2$. The mica was subsequently rinsed and images were recorded using 300 µl of recording buffer: 10 mM Tris–HCl pH 7.5, 150 mM KCl. Standard silicon nitride cantilevers (ThermoMicroscopes, CA, USA) with a length of 85 µm, force constant 0.5 N m^{-1} and operating frequencies 25–35 kHz (in liquid) were used as probe. High-resolution AFM images were obtained using tapping mode in liquid with a free amplitude of 2–5 nm and amplitude setpoint adjusted to minimal forces (damping of the free amplitude was 10–20%).

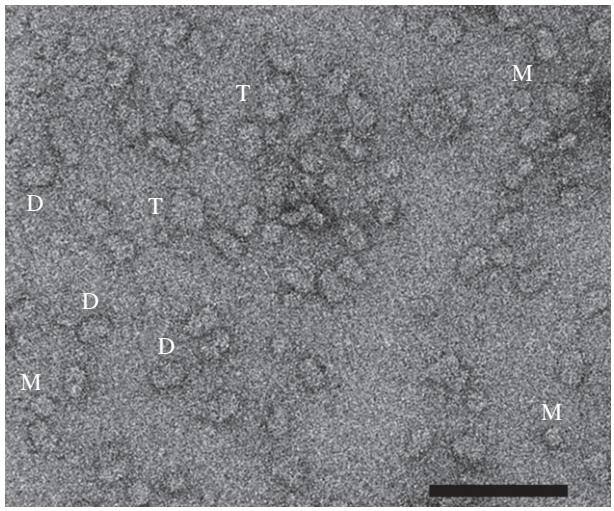

Figure 1. An image of negatively stained RC–LH1 particles of *Rhodobaca bogoriensis*. Some monomeric (M), dimeric (D) and tetrameric (T) molecules have been indicated. The scale bar equals 1000 Å.

3. RESULTS

(a) *Single-particle averaging of RC–LH1 dimers*

Inspection of EM images of negatively stained specimens of purified RC–LH1 complexes from *Rca. bogoriensis* showed monomeric, dimeric and tetrameric particles in a ratio of about 6 : 3 : 2 (figure 1). Because the monomer is a bit too small to be suitable for detailed single-particle analysis, efforts were focused on the dimers and tetramers. A total of 85 000 single-particle projections of RC–LH1 were collected. After an initial cycle of single-particle analysis and classification, the dimers could be divided into four subgroups, according to four preferential positions of association to the carbon film. In the two extreme positions, the dimer is seen in a top-view position, as in the plane of the membrane, and in a side-view position, vertical to the membrane. The other two subgroups show the dimer in intermediate positions. The tetramers could be divided into two subgroups as well.

About 24 000 particle projections originate from dimers in a top-view position, as in the plane of the membrane. The final map was obtained without imposing symmetry during analysis, but because two-fold rotational symmetry was very obvious, it was imposed afterwards (figure 2*a*). The smallest relevant details expected to be seen at the obtained resolution (13 Å) are the projected α helices. Although α helices measure typically about 10–12 Å in diameter, the association of two Bchl *a* molecules at the interface α- and β-subunits of the LH1 units leads to a 14 Å separation of the helices (centre-to-centre distance) [28]. Indeed, the two-dimensional map has many small peripheral densities of this size, surrounding

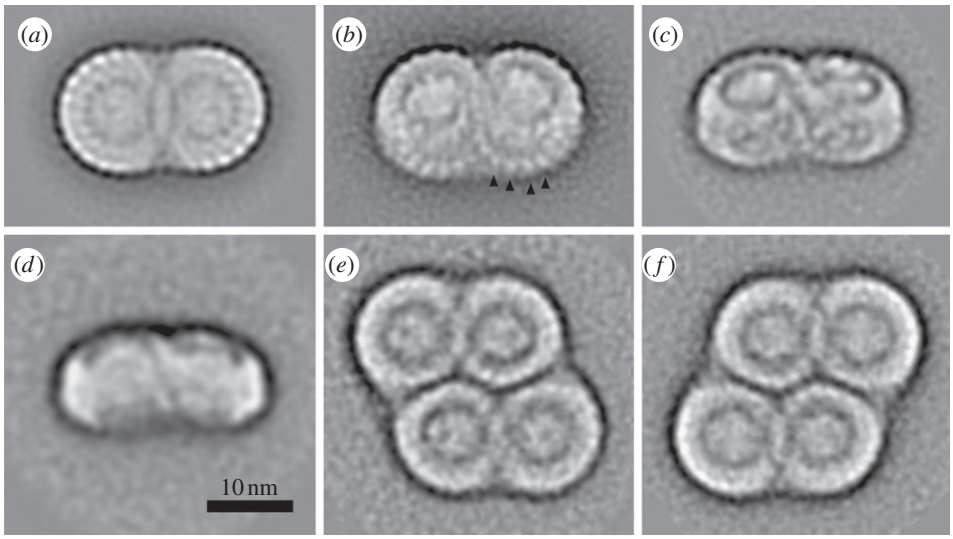

Figure 2. Average projection maps of RC–LH1 complexes, obtained from processing of about 75 000 single-particle projections. (*a*) Map of dimeric particles in a top-view position, as seen in the membrane plane. (*b*,*c*) Dimer maps of particles in a slightly and strongly tilted position, respectively. (*d*) Map of dimers in side-view position. (*e*,*f*) Two maps of tetrameric particles in top-view position. The maps result from particles that differ in handedness (face-up and face-down), resulting from a different attachment to the carbon support film.

two RCs. The ribbon of LH1 units appears, however, to be discontinuous at four positions close to the interface of the two halves of the complex.

Further analysis was performed separately on the three sets of slightly and strongly tilted complexes. These sets included a total of about 50 000 projections. The most detailed map was obtained from particles in a slightly tilted (10–20°) position (figure 2*b*). It shows a string of small stain excluding densities (see black arrowheads), which are the tips of the α helices of the LH1 units. Although they are seen from a side, the helices do not appear as long solid rods in this particular projection map. The obvious reason why they are not contrasted over the full length is the lack of penetration of the uranyl acetate negative stain inside the hydrophobic regions of membrane proteins. Figure 2*c* shows the RC–LH1 structure in a stronger tilted view, and it is obvious that the RC hardly sticks out of the LH1 ring. Figure 2*d* shows the RC–LH1 complex in a side-view position, in which the two halves of the dimer incline towards each other. They make an angle of 156°, in the same way as previously observed in *Rba. sphaeroides* [15]. The unusual angular shape of the dimers leads to a local curvature of the membrane, which is considered to increase the effective surface area for light gathering.

(b) *Single-particle averaging of RC–LH1 tetramers*

In total, a number of 10 000 tetrameric RC–LH1 single-particle projections were collected and processed. Classification of the projections indicated that the dataset consists of two distinct groups; the two final projection maps are presented in figure 2*e*,*f*. Inspection shows that both maps are from the same type of tetramer, but with a different handedness. This indicates that the RC–LH1 particles are attached in about equal numbers in two ways (up and down) to the carbon support film, in contrast to the single dimers where only one type of handedness was found. The tetramers appear to be composed of identical dimers and are considered to be the remnants of ribbons of dimers because occasionally particles consisting of three to four dimers were observed (not shown). Longer ribbons were seen in freeze-fracture images of intact, native membranes of *Rca. bogoriensis* (see below). They have also been detected before in AFM studies of *Rba. sphaeroides* [16]. In the tetramers, the dimers are not in an exactly vertical position, because the long and short axes of the ribbon make an angle of 68° (figure 2*e*,*f*). Because the maps of individual dimers show a twofold rotation symmetry, the tetramer is by definition also a symmetrical particle, and hence the symmetry was imposed in one of the final maps (figure 2*f*).

(c) *Interpretation of RC–LH1 projection maps*

Before performing a close analysis of the dimer projection map, it is of relevance to determine its absolute handedness. For this reason, we further processed the maps of the tetramer. The tetramer of figure 2*f* was mirrored and combined with the one of 2*e*. Both dimers of the tetramer were combined and twofold symmetry was imposed, leading to an eightfold increase in the signal in the map of figure 3*a*, when compared with figure 2*f*. Figure 3*a* shows at much better signal to noise level the four openings of the LH1 per dimer, although at slightly lower resolution as compared to figure 2*a*, probably because there are some angular differences in the attachment of the dimers in the up and down way to the support film, leading to a slight mismatch in positions after flipping. The increase in overall signal, however, allows a close comparison between the RCs of the tetramer (upper box in figure 3*a*) and the dimer map of figure 2*a* (lower box in figure 3*a*). Details of the motifs are at identical positions (upper and lower asterisks), pointing to the same handedness.

Freeze-fracture EM images of intact membranes of *Rca. bogoriensis* show a close packing of rows in which

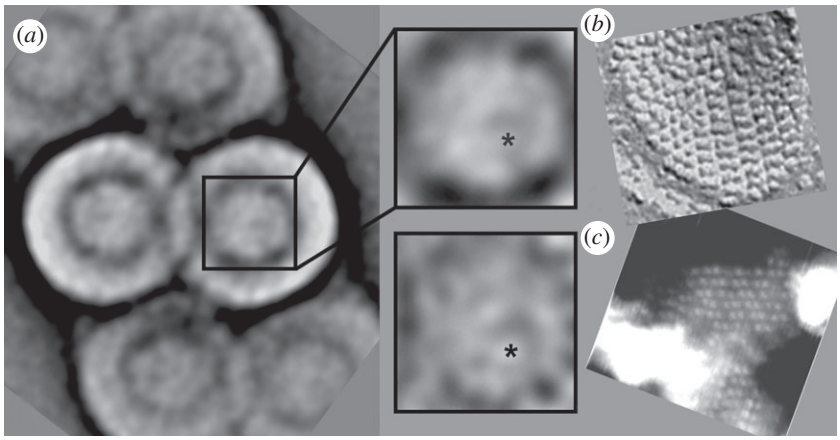

Figure 3. Relation between the tetramers and dimers and orientation of dimers in ribbons in the intact photosynthetic membrane. (*a*) Combined map of all dimers from the tetramers inclining to the left and right (after mirroring this image), with imposed twofold symmetry. The upper box shows the RC part at larger magnification for comparison with the same RC part of the dimer map from figure 2*a* (lower box). Asterisks show densities at similar positions in both maps. (*b*) Freeze-fracture electron microscopy image of intact membranes from *Rca. bogoriensis*, presented in a similar orientation as the tetramers from frame (*a*). (*c*) AFM image of tubular membranes of *Rba. sphaeroides*, faced from the cytoplasmic side of the plasma membrane.

the stacking of dimers inclines to the left (figure 3*b*). A same type of stacking has been observed by AFM in tubular membranes of an LH2 mutant of *Rba. sphaeroides* (see [29] for further details). The stacking makes a clear inclination (figure 3*c*), although not with exactly the same angle as in *Rca. bogoriensis*. Because in the latter membranes the membrane-exposed part of the H subunit protrudes the membrane in an upwards way, the AFM images give a direct clue for the absolute handedness. This makes it possible to merge the high-resolution structure of the RC into the dimer map of figure 2*a* in a way as presented in figure 4*a*.

In an attempt to assign the full peripheral antenna of the RC–LH1 dimers, we have marked the positions of all the bright peripheral densities by keeping in mind that pairs of them form an LH1 unit, with a maximal length of about 30 Å in projection. In one-half of the RC–LH1 dimer the map contains 13 outer β-subunits (marked by orange circles 1–13, figure 4*a*) and 13 inner α-subunits (green circles 1–13). Only two of them cannot be distinguished in the map (marked by fuzzy orange and green rings). The interface is composed of a rather featureless elongated density, in which helices are not separated as well. But if we consider the surface of the interface, it will accommodate another four helices (blue circles, figure 4*a*). On both sides of the right RC, a gap of 35 Å remains between the helices marked by blue and green circles, which is partly occupied by a cleft. Next to the cleft, between the two extreme, α-subunits of the LH1 ring and the RC, are two densities with an elongated size (marked red), and these two densities have the right size to be occupied by PufX copies. The *Rca. bogoriensis* strain LBB1 contains a PufX subunit homologous to *Rba. sphaeroides*, as found by PCR and mass spectrometry characterization (see §2). An elongated projection of PufX makes sense, because recently the PufX structure was proposed to be composed of a vertically positioned membrane-inserted helix plus a horizontal, peripheral helix [19].

The projection map of the tilted dimer gives further evidence that the earlier-proposed interpretation of helices is valid, because the densities of the 13 outer β-subunits can be seen at the same inter-subunit distance (see orange arrowheads in figure 4*b* and orange circles in figure 4*a*). In fact, we see only the tips of the helices, because the negatively stained specimens do not reveal much of the interior of the complex, as discussed earlier. Besides, the maps have excellent resolution, because it can be seen in the tilted dimer map that some of the tips of the helices do not overlap anymore. The tips of the α- and β-subunits of LH1 unit 6 can be seen as four densities instead of two (figure 4*b*). Except for unit 6, we can deduce at the circumference the positions of all the β-subunits from the densities in a straightforward way. Helices of subunits 11–13 appear closer than those of 7–10, in both the tilted map (orange arrowheads, figure 4*b*) and the non-tilted map (orange circles, figure 4*a*). Furthermore, in the tilted view, the α-subunit of LH1 unit 1 is clearly visible (green arrowhead). Next to this helix is the helix assigned to PufX (red arrowhead). Finally, in the upper part of the tilted view, the cleft is plain to see (marked by the blue bar), and next to it we see a continuous density between the LH1 ring and the RC. This connection is proposed to be occupied by the horizontal helix of PufX.

4. DISCUSSION

Single-particle EM was performed on RC–LH1–PufX complexes of *Rca. bogoriensis* with the aim of establishing the peripheral antenna conformation, and in particular the structural role of PufX. We have chosen the negative staining technique to prepare the RC–LH1 complexes, rather than cryo-EM, because it gives a higher contrast. Maps were obtained at a resolution of 13 Å, in which the tips of the α helices of the LH1 units could be resolved. The dimer map shows the positions of 13 LH1 units in each half ring plus another two in the interface, bringing the total for the dimer to 2×14. A similar number was previously found in a study of two-dimensional crystals of *Rba. sphaeroides* RC–LH1 at a resolution of 8.5 Å [11]. The new map shows the RC in a similar

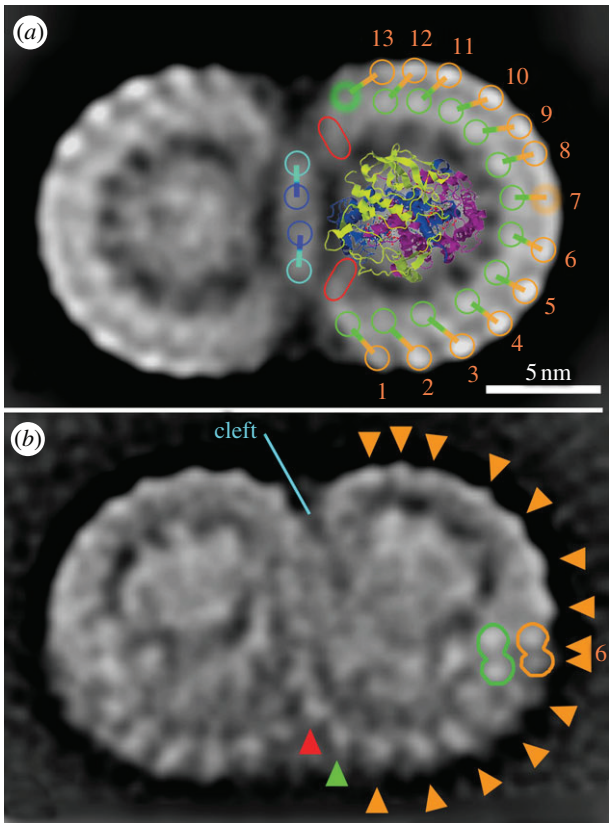

Figure 4. (*a*) Assignment of the dimer map of *Rca. bogoriensis* RC–LH1. Components have been indicated in one half dimer plus the full interface. The centre is occupied by one RC with the peripheral part of the H subunit (yellow) on top of the L (magenta) and M (blue) subunits. The periphery contains 13 LH1 (numbered 1–13), composed of α- and β-subunits (green and orange circles, respectively), plus two PufX subunits (red) and the one additional LH1 unit in the RC (blue). (*b*) Further evidence for the helix assignment in the non-tilted projection map of (*a*) from a slightly tilted map, presented in figure 2*b*. Orange arrowheads point to the same helices as numbered 1–13. The green arrowhead points to the α-subunit of LH1 unit 1 and the red arrowhead to the transmembrane part of the PufX subunit. The tips of the helices of LH1 unit 6 do not overlap (double arrowheads).

position if all three dimensions are considered, with the water-exposed domain of the H subunit oriented in an upwards position.

There are, however, some notable differences between *Rca. bogoriensis* and *Rba. sphaeroides*. First, the LH1 ribbon of the latter is continuous in the form of an S, with two PufX subunits next to the ends of the ribbon. In *Rca. bogoriensis*, the ribbon is broken into two half-circles and a third piece of the string is formed by two LH1 units at the interface. Second, in our study, the map indicates space for four PufX molecules, instead of two. The position of the peripheral membrane helix of the lower PufX subunit is clearly depicted in the non-tilted dimer by a bridge between LH1 and the RC (figure 4*a*), and the membrane-intrinsic helical part of the lower PufX is visible in the tilted map (red triangle, figure 4*b*). The peripheral helix of the upper PufX is plain to see in the tilted dimer (figure 4*b*), but also in the tetramer map after summing the four independent dimers and imposing symmetry (figure 3*a*). The fact that this small horizontal helix is visible has much to do with the application of the negative staining technique, because the stain does not contrast the innermost parts of the RC–LH1 complex, which otherwise could have lowered the signal in a full projection of the structure, as is the case in cryo-EM.

The presented model is another addition to the list of propositions for the RC–LH1–PufX structure, but is at least based on direct structural data, in contrast to the general model for *Rhodobacter* species of Busselez *et al.* [5], which proposes a dimer with 2 × 12 LH1 units connected to a central PufX monomer. This model was inspired from extrapolating the three-dimensional structure of the monomeric complex of *Rba. veldkampii*. Our model is the first where the LH1–PufX ribbon is discontinuous. In all other models, the LH1 ribbon looks like one long string with the shape of the letter S, as is seen in our slightly tilted map of figure 4*b* by overlap of the densities. The highest detailed map of *Rba. sphaeroides* at 8.5 Å resolution assigns positions of α helices in a continuous band around the interface [11], although some densities are very faint (fig. 2*b*, red dots near the red open circles in Qian *et al.* [11]) at places where in our map the strings are discontinuous. This does not mean, however, that the two detailed models are in conflict. It is very well possible that there are slight differences between species about the precise arrangement of the LH1 and PufX subunits in the RC–LH1 dimers. If this is the case, spectroscopy could shed light on the differences in the ribbons, because continuous and discontinuous strings should have a different excitonic behaviour. Advanced spectroscopy may also shed light on the question whether PufX binds chlorophyll, as discussed in a recent review [14].

The finding that there are additional densities that can be assigned to PufX helices next to the four openings of the LH1 ribbon prompted us to assign 2 × 2 PufX proteins in the model. The PufX to RC stoichiometry was determined before any structure of a RC–LH1 dimer was established in *Rba. sphaeroides* by Western blot analysis. A PufX/RC ratio of 0.86–0.99 was found [18], which points to a 1 : 1 stoichiometry. *Rhodobaca bogoriensis* has a PufX protein with a determined sequence (C. Jungas 2011, unpublished data), but the stoichiometry is not known. Not only the number of copies but also the position of the PufX molecules is in contrast to other models. In one of them, the interaction between the PufX polypeptide and LH1 subunits is based on a calculation from a molecular dynamics flexible fitting simulation of the RC–LH1 dimer, using a conformer of PufX from the determination of the solution structure with an extended N-terminus [19]. It shows the horizontal α helices of the two PufX proteins point towards the centre of the interface superimposing the LH1 ribbon. In contrast, our maps of dimers and tetramers do not show such masses connecting the two LH1 units at the interface.

The functional significance of the dimeric and the novel tetrameric structures is an interesting theme. Previous connectivity studies on isolated RC–LH1 dimers suggest that the dimers constitute a privileged structure for antenna connectivity. We have shown that the availability of the excitation from a monomer with a closed RC to the other monomer is perfect, meaning that the LH1-to-LH1 transfer is not

rate-limiting with respect to the LH1-to-RC transfer [22]. The tetramers result from a supra-organization of dimers in the membrane. Only one type of association was found in which the dimers tend to be organized in rows that are several dimers long. The function of this organization is likely to facilitate easier quinone flow in conditions where the quinone pool is predominantly reduced, as happens under photosynthetic conditions.

5. OUTLOOK

In principle, all remaining uncertainties about structural details of the RC–LH1, such as the precise number of PufX molecules and their location, could be solved from a high-resolution structure. EM is well able to resolve a protein structure to near-atomic resolution and to provide electron density maps that allow a close fit of amino acid side chains. But such structures have been mostly solved with water-soluble macromolecular complexes, such as viruses [30], or were performed with two-dimensional crystals [31]. The highest resolution structure obtained by single-particle analysis for a membrane protein is a 9.7 Å structure of a V-type ATPase [32]. The large hydrophilic domains were particularly helpful in the three-dimensional reconstruction process. The purple bacterial RC–LH1–PufX dimer is smaller and rather flat and will be harder to solve at such a resolution. Ultimately, the cryo-EM method is likely to be the best way of extending present knowledge, as presented in this study.

This work was supported by the HARVEST Marie Curie Research Training Network (PITN-GA-2009-238017). We thank Dr M.T. Madigan for the kind gift of *Rca. bogoriensis*, strain LBB1. We gratefully acknowledge the contribution of Marseille Protéomique-CNRS-Aix Marseille Université (Sabrina Lignon, Mathilde Joint and Régine Lebrun from the Institut de Microbiologie de la Méditerranée, FR3479; Maya Belghazi from the Centre d'Analyses Protéomiques CRN2M-UMR 7286) for mass spectrometry analyses. Many thanks also to Dr Arjan de Groot for PCR analysis of *Rca. bogoriensis* and Drs Neil Hunter and John Olsen for preparation of membranes used in AFM experiments.

REFERENCES

1 Law, C. J., Roszak, A. W., Southall, J., Gardiner, A. T., Isaacs, N. W. & Cogdell, R. J. 2004 The structure and function of bacterial light-harvesting complexes. *Mol. Membr. Biol.* **21**, 183–191. (doi:10.1080/09687680410001697224)

2 Jay, F., Lambillotte, M., Stark, W. & Mühlethaler, K. 1984 The preparation and characterization of native photoreceptor units from the thylakoids of *Rhodopseudomonas viridis*. *EMBO J.* **3**, 773–776.

3 Roszak, A. W., Howard, T. D., Southall, J., Gardiner, A. T., Law, C. J., Isaacs, N. W. & Cogdell, R. J. 2003 Crystal structure of the RC-LH1 core complex from *Rhodopseudomonas palustris*. *Science* **302**, 1969–1972. (doi:10.1126/science.1088892)

4 Boonstra, A. F., Germeroth, L. & Boekema, E. J. 1994 Structure of the light harvesting antenna from *Rhodospirillum molischianum* studied by electron microscopy. *Biochim. Biophys. Acta* **1184**, 227–234. (doi:10.1016/0005-2728(94)90227-5)

5 Busselez, J., Cottevieille, M., Cuniasse, P., Gubellini, F., Boisset, N. & Lévy, D. 2007 Dimerization of photosynthetic core complexes. *Structure* **15**, 1674–1683. (doi:10.1016/j.str.2007.09.026)

6 Liu, L. N., Sturgis, J. N. & Scheuring, S. 2011 Native architecture of the photosynthetic membrane from *Rhodobacter veldkampii*. *J. Struct. Biol.* **173**, 138–145. (doi:10.1016/j.jsb.2010.08.010)

7 Fotiadis, D., Qian, P., Philippsen, A., Bullough, P. A., Engel, A. & Hunter, C. N. 2004 Structural analysis of the reaction center light-harvesting complex I photosynthetic core complex of *Rhodospirillum rubrum* using atomic force microscopy. *J. Biol. Chem.* **279**, 2063–2068. (doi:10.1074/jbc.M310382200)

8 Crouch, L. I. & Jones, M. R. 2012 Cross-species investigation of the functions of the *Rhodobacter* PufX polypeptide and the composition of the RC–LH1 core complex. *Biochim. Biophys. Acta* **1817**, 336–352. (doi:10.1016/j.bbabio.2011.10.009)

9 Jungas, C., Ranck, J. L., Rigaud, J. L., Joliot, P. & Vermeglio, A. 1999 Supramolecular organization of the photosynthetic apparatus of *Rhodobacter sphaeroides*. *EMBO J.* **18**, 534–542. (doi:10.1093/emboj/18.3.534)

10 Scheuring, S., Francia, F., Busselez, J., Melandris, B. A., Rigaud, J.-L. & Lévy, D. 2004 Structural role of PufX in the dimerization of the photosynthetic core complex of *Rhodobacter sphaeroides*. *J. Biol. Chem.* **279**, 3620–3626. (doi:10.1074/jbc.M310050200)

11 Qian, P., Hunter, C. N. & Bullough, P. A. 2005 The 8.5Å projection structure of the core RC-LH1-PufX dimer of *Rhodobacter sphaeroides*. *J. Mol. Biol.* **349**, 948–960. (doi:10.1016/j.jmb.2005.04.032)

12 Scheuring, S., Busselez, J. & Lévy, D. 2005 Structure of the dimeric PufX-containing core complex of *Rhodobacter blasticus* by in situ atomic force microscopy. *J. Biol. Chem.* **280**, 1426–1431. (doi:10.1074/jbc.M411334200)

13 Deisenhofer, J., Epp, O., Miki, K., Huber, R. & Michel, H. 1985 Structure of the protein subunits in the photosynthetic reaction centre of *Rhodopseudomonas viridis* at 3 Å resolution. *Nature* **318**, 618–624. (doi:10.1038/318618a0)

14 Holden-Dye, K., Crouch, L. I. & Jones, M. R. 2008 Structure, function and interactions of the PufX protein. *Biochim. Biophys. Acta* **1777**, 613–630. (doi:10.1016/j.bbabio.2008.04.015)

15 Qian, P., Bullough, P. A. & Hunter, N. 2008 Three-dimensional reconstruction of a membrane-bending complex: the RC–LH1–PufX core dimer of *Rhodobacter sphaeroides*. *J. Biol. Chem.* **283**, 14 002–14 011. (doi:10.1074/jbc.M800625200)

16 Bahatyrova, S. *et al.* 2004 The native architecture of a photosynthetic membrane. *Nature* **430**, 1058–1062. (doi:10.1038/nature02823)

17 Recchia, P. A., Davis, C. M., Lilburn, T. G., Beatty, J. T., Parkes-Loach, P. S., Hunter, C. N. & Loach, P. A. 1998 Isolation of the PufX protein from *Rhodobacter capsulatus* and *Rhodobacter sphaeroides*: evidence for its interaction with the alpha-polypeptide of the core light-harvesting complex. *Biochemistry* **31**, 11 055–11 063. (doi:10.1021/bi980657l)

18 Francia, F., Wang, J., Venturoli, G., Melandri, B. A., Barz, W. P. & Oesterhelt, D. 1999 The reaction center-LH1 antenna complex of *Rhodobacter sphaeroides* contains one PufX molecule which is involved in dimerization of this complex. *Biochemistry* **38**, 6834–6845. (doi:10.1021/bi982891h)

19 Ratcliffe, E. C., Tunnicliffe, R. B., Ng, I. W., Adams, P. G., Qian, P., Holden-Dye, K., Jones, M. R., Williamson, M. P. & Hunter, C. N. 2011 Experimental evidence that the membrane-spanning helix of PufX adopts a bent conformation that facilitates dimerisation of the *Rhodobacter sphaeroides* RC–LH1 complex through

N-terminal interactions. *Biochim. Biophys. Acta* **1807**, 95–107. (doi:10.1016/j.bbabio.2010.10.003)
20 Hsin, J., LaPointe, L. M., Kazy, A., Chipot, C., Senes, A. & Schulten, K. 2011 Oligomerization state of photosynthetic core complexes is correlated with the dimerization affinity of a transmembrane helix. *J. Am. Chem. Soc.* **133**, 14 071–14 081. (doi:10.1021/ja204869h)
21 Milford, A. D., Achenbach, L. A., Jung, D. O. & Madigan, M. T. 2000 *Rhodobaca bogoriensis* gen. nov. and sp. nov., an alkaliphilic purple nonsulfur bacterium from African Rift Valley soda lakes. *Arch. Microbiol.* **174**, 18–27. (doi:10.1007/s002030000166)
22 Comayras, R., Jungas, C. & Lavergne, J. 2005 Functional consequences of the organization of the photosynthetic apparatus in *Rhodobacter sphaeroides*. *J. Biol. Chem.* **280**, 11 214–11 223. (doi:10.1074/jbc.M412089200)
23 Tsukatani, Y., Matsuura, K., Masuda, S., Shimada, K., Hiraishi, A. & Nagashima, K. V. 2004 Phylogenetic distribution of unusual triheme to tetraheme cytochrome subunit in the reaction center complex of purple photosynthetic bacteria. *Photosynth. Res.* **79**, 83–91. (doi:10.1023/B:PRES.0000011922.56394.92)
24 Oostergetel, G. T., Keegstra, W. & Brisson, A. 1998 Automation of specimen selection and data acquisition for protein electron crystallography. *Ultramicroscopy* **74**, 47–59. (doi:10.1016/S0304-3991(98)00022-9)
25 Van Heel, M. 1987 Similarity measures between images. *Ultramicroscopy* **21**, 95–100. (doi:10.1016/0304-3991(87)90010-6)
26 Abramoff, M. D., Magalhaes, P. J. & Ram, S. J. 2004 Image processing with ImageJ. *Biophotonics Int.* **11**, 36–42.
27 Van der Werf, K. O., Putman, C. A. J., de Grooth, B. G., Segerink, F. B., Schipper, E. H., Van Hulst, N. F. & Greve, J. 1993 Compact stand-alone atomic force microscope. *Rev. Sci. Instrum.* **64**, 2892–2897. (doi:10.1063/1.1144378)
28 Wang, Z. Y., Gokan, K., Kobayashi, M. & Nozawa, T. 2005 Solution structures of the core light-harvesting alpha and beta polypeptides from *Rhodospirillum rubrum*: implications for the pigment–protein and protein–protein interactions. *J. Mol. Biol.* **347**, 465–77. (doi:10.1016/j.jmb.2005.01.017)
29 Bahatyrova, S. 2005 Atomic force microscopy of bacterial photosystems: a new model for native membrane organization. PhD thesis, University of Twente, The Netherlands.
30 Zhang, X., Jin, L., Fang, Q., Wong, H. H. & Zhou, Z. H. 2010 3.3 Å cryo-EM structure of a nonenveloped virus reveals a priming mechanism for cell entry. *Cell* **141**, 472–482. (doi:10.1016/j.cell.2010.03.041)
31 Henderson, R., Baldwin, J. M., Ceska, T. A., Zemlin, F., Beckmann, E. & Downing, K. H. 1990 Model for the structure of bacteriorhodopsin based on high-resolution electron cryomicroscopy. *J. Mol. Biol.* **213**, 899–929. (doi:10.1016/S0022-2836(05)80271-2)
32 Lau, W. C. Y. & Rubinstein, J. L. 2012 Subnanometre-resolution structure of the intact *Thermus thermophilus* H^+-driven ATP synthase. *Nature* **481**, 214–218. (doi:10.1038/nature10699)